JCTC Journal of Chemical Theory and Computation

# Electronic Structure Calculation of MgO (001) Surface with Aggregated Oxygen Vacancies

Motoi Tobita* and Shirun Ho

*Hitachi, Ltd., Advanced Research Laboratory (ARL), 1-280 Higashi-Koigakubo, Kokubunji-shi, Tokyo 185-8601, Japan*

Received November 8, 2007

**Abstract:** The electronic structure of an MgO (001) surface with aggregated oxygen vacancies at the surface was investigated by using a density-functional embedded-cluster method using $Mg_{45}O_x$ ($x = 39-45$) clusters and the B3LYP/CEP-121G level of calculation. The investigation found that the distribution of energy levels corresponding to oxygen-vacancy states strongly depends on the number and configuration of oxygen vacancies. Molecular orbitals of the oxygen vacancy states consist of orbitals at the vacancy sites and their neighboring magnesium ions. These orbitals can simply be modeled by orbitals formed from interacting pseudoatoms. A pseudoatom is an electronically neutral atom representing an oxygen vacancy and electrons of magnesium ions near the vacancy. With this model, an *N*-atom system having *n* vacancies can be modeled by *n* pseudoatoms. Interactions among oxygen vacancies in MgO were qualitatively reproduced by the interacting pseudoatoms model.

## Introduction

Magnesium oxide (MgO) is an important material in many industrial applications. A perfect crystal of MgO has a NaCl-like structure and features hardness, transparency, and good insulating properties. In MgO materials, as in other oxides, vacancies are often present. Vacancies alter optical and electronic properties significantly from those observed in the perfect crystal. MgO can therefore be engineered in order to meet a specific need by controlling the position, charged state, and density of vacancies. The secondary-electron-emission coefficient is an example of a property that strongly depends on the position, charged state, and density of oxygen vacancies.[1] This coefficient can be approximately calculated as a function of several parameters including valence-bandwidth, energy levels of the oxygen-vacancy states, band gap, and electron affinity.[2]

Some of the above parameters have been obtained in prior experimental[1,3–11] and theoretical[11–22] investigations. Optical-absorption measurements[1,3,4] showed that the band gap of bulk MgO is 7.4−7.8 eV. Systems with an oxygen mono-vacancy (called F-center or $F^+$-center) with a trapping charge of −2 or −1, respectively, have been studied, and the vacancy energy level has been identified by luminescence measurements.[5–10] *Ab initio* calculations of oxygen vacancies as well as structural and energetic investigations have been done for bulk and surface MgO.[13–23]

On the other hand, much less is known about MgO with aggregated oxygen vacancies, which is the subject of the current paper. Experimentally, aggregated vacancies have been observed in many materials by surface reconstruction driven by annealing (see ref 18 and references therein). Using semiempirical complete neglect of differential overlap calculations, Castanier and Noguera predicted that aggregated oxygen vacancies are energetically more favored over periodically spread oxygen vacancies.[15] Finocchi et al. theoretically investigated interaction between oxygen vacancies using the local density approximation (LDA) functional under the periodic boundary condition (PBC).[18] Their calculations used pseudopotential for core electrons. The wave function of valence electrons was expanded by using a plane-wave basis set. They calculated vacancy-formation energy as a function of concentration and configuration of vacancies and derived a two-body model potential accounting for interaction between vacancies.

The LDA functional performed well in predicting equilibrium geometry and vibrational frequencies of corundum ($\alpha$-$Al_2O_3$).[24] However, LDA is not the best method for

* Corresponding author e-mail: motoi.tobita.mb@hitachi.com.

10.1021/ct700303v CCC: $40.75 
Published on Web 06/14/2008

predicting band gaps. Therefore, the previous energy levels calculated by LDA are of only qualitative importance.

In this study, density-functional-theory calculations were performed on finite-size clusters of MgO embedded in the crystalline electrostatic potential. In the calculation, core electrons are described by the pseudopotential, as done in the previous LDA study. The wave function of valence electrons is expanded by a linear combination of atomic orbitals. The exchange-correlation term is evaluated by using the B3LYP functional,[25,26] which is known to predict band gaps of a variety of materials, typically within an error of a few tenths of an electronvolt when a large enough basis set is used. Examples of band gap calculations include polypeptides,[27] polyynes,[28] molecular crystals,[29] and metal oxides.[30] The success of the B3LYP functional is due to the correction of the self-interaction error inherent in the LDA and in the generalized gradient approximation functional by a mixing of Hartree-Fock exchange in B3 exchange functional form.[25] The B3LYP functional is thus expected to better predict energy levels of MgO with various oxygen-vacancy configurations. The embedded-cluster model defines an MgO structure with locally aggregated oxygen vacancies. The bulk-size effect, which is important in calculations of ionic materials such as MgO, is approximately included in the model by using embedding-electrostatic potentials.

In this study, orbital-energy-related quantities such as valence-bandwidth, energy levels of oxygen-vacancy states, band gap, and electron affinity of an MgO (001) surface with aggregated oxygen vacancies were calculated. For comparison, calculations were also performed for bulk MgO, an MgO perfect surface, and a surface F-center. It was found that, when oxygen vacancies aggregate, vacancy energy levels split, and the amount of split depends on the number of oxygen-vacancy pairs separated by the nearest-neighbor oxygen distance. The main components of molecular orbitals corresponding to the oxygen-vacancy states are located at oxygen-vacancy sites. An oxygen-vacancy site can thus be viewed as a pseudoatom. Indeed, a system where each oxygen vacancy site is represented by a helium atom reproduces the shape and energy-ordering of molecular orbitals corresponding to the oxygen-vacancy states of MgO with aggregated oxygen vacancies.

In summary, MgO with aggregated oxygen vacancies can exhibit significantly different optical and electronic properties as compared with MgO with monovacancies. Thus, secondary-electron-emission phenomena should largely be influenced by the size and density of surface oxygen vacancies of a material.

## Methods

**A. Modeling.** *1. Embedded-Cluster Model.* The MgO crystal structure has a NaCl-type cubic lattice with a lattice constant of 4.2112 Å. In our calculations, MgO was modeled by finite-size rectangular parallelepiped clusters, where (001) is exposed at each face of the rectangular parallelepiped. The clusters were embedded in a box of point charges that mimicked the Madelung potential made by an ionic crystal lattice. The effect of point charges on the quantum-chemically treated cluster was included in the Hamiltonian through one-electron integrals.

Bulk MgO was also modeled, as well as the MgO surface, to clarify the effect on the surface. In the bulk-MgO model, the cluster was embedded in the center of the point-charge box; however, in the MgO-surface model, the cluster was embedded in the center of the top surface of the point-charge box. The positions of the point charges were fixed at magnesium and oxygen sites of the MgO perfect crystal. The effects of two different types of point-charge quantities, that is, formal charge and consistent charge,[31] were compared. The formal-charge quantity is +2.0 for point charges at magnesium sites and −2.0 for those at oxygen sites. The consistent charge was determined so that the point-charge quantity at each magnesium site is equal to the average of Mulliken-charge quantities on the Mg atoms of the cluster. The size of the point-charge box was fixed at $15 \times 16 \times 13$ for the bulk MgO and $15 \times 16 \times 8$ for the MgO surface. With these box sizes, the calculated orbital-energy-related quantities converged to 0.01 eV.

*2. Cluster Structure.* Convergence of the orbital-energy-related quantities with respect to the cluster size was investigated using six different sizes of rectangular parallelepiped clusters: $1 \times 2 \times 1$ (MgO), $3 \times 4 \times 2$ ($Mg_{12}O_{12}$), $5 \times 6 \times 3$ ($Mg_{45}O_{45}$), $5 \times 6 \times 4$ ($Mg_{60}O_{60}$), $7 \times 8 \times 3$ ($Mg_{84}O_{84}$), and $7 \times 8 \times 4$ ($Mg_{112}O_{112}$). In this model, the third parameter $z$ of "$x \times y \times z$" represents layer thickness. These cluster sizes satisfy the conditions recommended by Lü et al.; namely, in cluster calculations of metal oxides, the cluster should be charge-neutral and stoichiometric.[32]

Effects of geometry relaxation on the orbital-energy-related quantities were investigated using clusters possessing one, three, or five oxygen vacancies, where each of them traps a charge of −2. These cluster structures were constructed by removing oxygen atoms from the charge-neutral and stoichiometric $7 \times 8 \times 3$ cluster surface. The considered structures are depicted in Figure 1a. In the force calculation during geometry relaxation, interactions between an atom and a point charge were described by the electrostatic potential made by the point charge with an additional electron-repulsion potential of the exponential form

$$A \exp(-r/\rho)$$

where $\rho$ is an nonbonded interaction parameter, $r$ is the distance between a point charge and an atom, and $A$ is a proportional parameter. The values of $\rho$ and $A$ that are used are 0.252 $Å^{-1}$ and 18065.8 kcal/mol for point charges at magnesium sites and 0.26 $Å^{-1}$ and 58298.9 kcal/mol for those at oxygen sites, respectively.[33]

Clusters possessing two to six oxygen vacancies, where each of them traps a charge of −2, were constructed by removing two to six oxygen atoms from the charge-neutral and stoichiometric $5 \times 6 \times 3$ cluster surface. The geometry of the remaining atoms was fixed at the perfect crystal structure, and the point-charge quantity was fixed at the formal charge values. The considered structures, including the perfect surface and the surface F-center, are depicted in Figure 1b. The number included in each structure label shows the number of oxygen vacancies in the cluster.

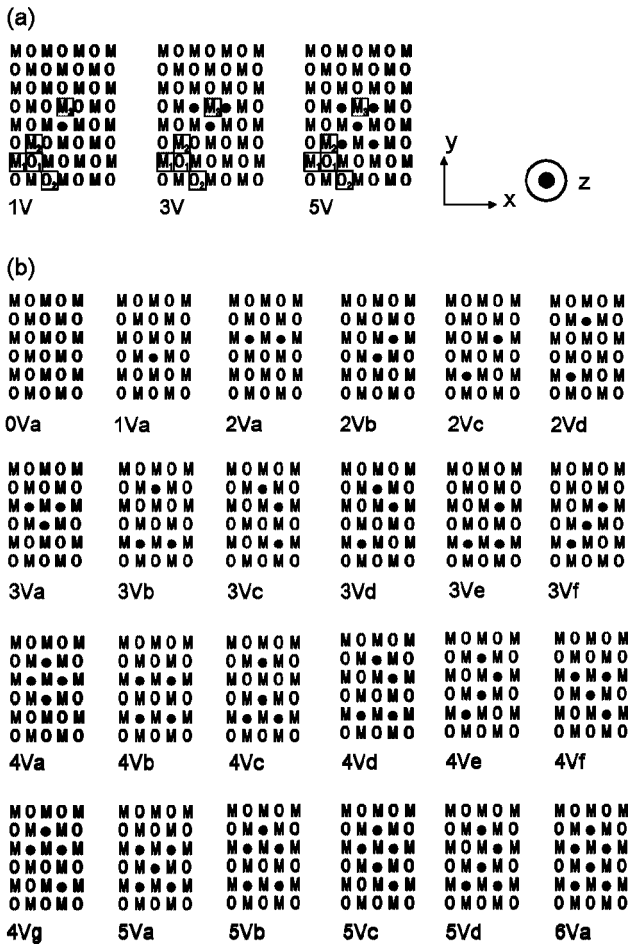


***Figure 1.*** Structures of MgO clusters investigated. (a) 7 × 8 × 3 clusters with one, three, or five oxygen vacancies. (b) 5 × 6 × 3 clusters with zero to six oxygen vacancies. Only the top layer is shown. The second and third layers include no oxygen vacancies; M, magnesium atom; O, oxygen atom; closed circle, oxygen vacancy with a trapping charge of −2.

**B. Calculation of Orbital-Energy-Related Quantities.** An initial investigation of cluster size and the geometry relaxation effect on the orbital-energy-related quantities was performed at the B3LYP[25,26]/CEP-4G[34] level of calculation. Further analyses were performed using a larger basis set at the B3LYP/CEP-121G[34] level. The B3LYP functional is a Hartree-Fock/pure-DFT hybrid functional. Its exchange term contains a 20% contribution from the Hartree-Fock exchange term. The CEP-4G and CEP-121G basis sets are an effective-core-potential basis set. Oxygen 1s electrons and magnesium 1s through 2p electrons are described by the effective core potential. In CEP-4G, valence electrons are expanded by one s-type function and a set of p-type functions. Whereas in CEP-121G, three s-type functions and three sets of p-type functions are used in the expansion. Although the B3LYP functional predicts the band gap of materials with good accuracy when a large enough basis set is used, the CEP-121G basis set is not large enough. To estimate orbital energies with the basis set limit, occupied energy levels ($E_{OCC}$) and the lowest unoccupied molecular orbital (LUMO) energy ($E_{LUMO}$) were corrected by using the following empirical relations

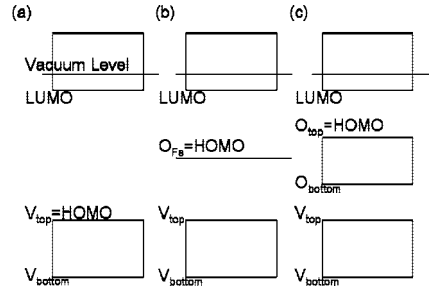


***Figure 2.*** Distribution of orbital energies for (a) perfect MgO, (b) MgO with surface F-center, and (c) MgO with aggregated oxygen vacancies at the surface.

derived for the highest occupied molecular orbital (HOMO) and LUMO energy correction:[35]

$$E_{OCC} = (E_{OCC}^{*} + 0.050)/1.001 \quad (1)$$

$$E_{LUMO} = 0.6091 E_{LUMO}^{*} - 0.475 \quad (2)$$

where energy terms with an asterisk are calculated quantities and terms without an asterisk are corrected quantities for the basis set limit. This kind of empirical correction is valid because using an incomplete basis set introduces a systematic error in orbital energies.[35–37] Note that the coefficients in the above relations are not optimized for B3LYP/CEP-121G, but for B3LYP/6-31G(d). We assume that these coefficients are still qualitatively "good" because the used functional is the same and because both basis sets are similar in terms of the number of functions per atom.

The calculated orbital energies were used to calculate the valence bandwidth as the energy difference between the top and bottom of the valence orbitals. Band gap was calculated as the energy difference between HOMO and LUMO. Electron affinity was calculated as the energy difference between the vacuum level and LUMO.

All of the calculations were performed using Gaussian03.[38]

## Results and Discussion

Before the calculated results are discussed, the orbital-energy distribution of MgO is briefly explained, using Figure 2. The energy distribution for a perfect MgO surface, MgO with a surface F-center, and MgO with aggregated oxygen vacancies at the surface is shown in Figure 2a−c, respectively. In all of the cases, LUMO lies below the vacuum level. Energy levels of oxygen-vacancy states lie in between the LUMO and the top of valence orbitals, $V_{top}$, as seen in Figure 2b,c. As a consequence, the top of the oxygen-vacancy levels becomes the HOMO when vacancies exist in the MgO.

**A. Initial Investigation of Cluster Size and Geometry Relaxation Effects.** The orbital-energy-related quantities of the MgO surface calculated with different sizes of cluster are given in Figure 3. Calculated orbital energy differences LUMO−HOMO, HOMO−$V_{bottom}$, and −LUMO were 5.85, 4.92, and −1.14 eV, respectively, when a 7 × 8 × 4 cluster was used. The energy differences obtained with a 5 × 6 × 3 cluster differed by 0.03 eV for LUMO−HOMO and −LUMO and by 0.3 eV for HOMO−$V_{bottom}$ as compared with the values obtained with the 7 × 8 × 4 cluster. From these data, we judged it suitable to perform further investiga-

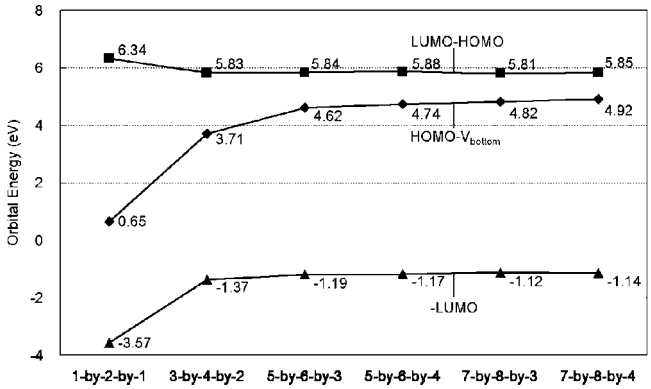


***Figure 3.*** Convergence of orbital-energy-related quantities with respect to cluster size calculated at the B3LYP/CEP-4G level.

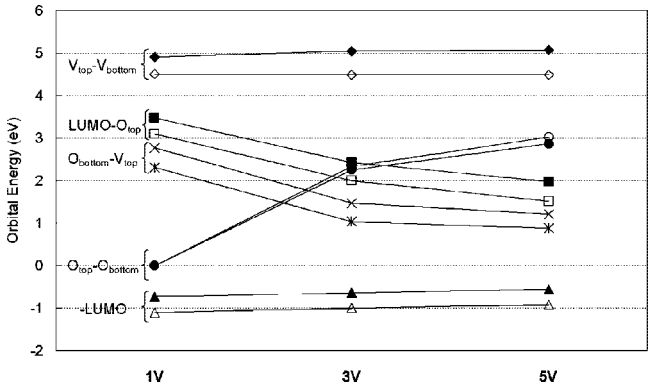


***Figure 4.*** Orbital energies of clusters having one, three, or five oxygen vacancies with and without geometry relaxation effects calculated at the B3LYP/CEP-4G level. Stars and closed diamonds, squares, circles, and triangles show values without geometry relaxation. Crosses and open diamonds, squares, circles, and triangles show values with geometry relaxation.

tions using the $5 \times 6 \times 3$ cluster. A prior investigation also supports the use of at least a three-layer model for a quantitative description of the surface F-center.[17]

The orbital-energy-related quantities of the MgO surface having one, three, or five oxygen vacancies with and without geometry relaxation effects are given in Figure 4. The amounts of shift in the energy differences are almost constant regardless of the number of oxygen vacancies. Those values between the top and bottom of the valence orbital ($V_{top}-V_{bottom}$), between the LUMO and the top of the oxygen vacancy orbital (LUMO$-O_{top}$), between the bottom of the oxygen vacancy orbital and the top of the valence orbital ($O_{bottom}-V_{top}$), and between the vacuum level and the LUMO ($-$LUMO) are all around 0.4$-$0.5 eV. The energy difference between the top and bottom of the oxygen vacancy orbital ($O_{bottom}-O_{top}$) is much less affected by the geometry relaxation effects. These results demonstrate that the contribution of the geometry relaxation effects to the orbital energy difference is small. Thus, further investigations (subsection B and later) using a larger basis set were performed using the perfect crystal structure. Geometries of systems with vacancies are constructed by simply deleting coordinates of atoms from those of the perfect crystal.

***Table 1.*** The Amount of Displacement from Crystalline Lattice for the Selected Atoms in Particular Direction after Geometry Relaxation (Å)[a]

| | | structure | | |
|---|---|---|---|---|
| atom | direction | 1V | 3V | 5V |
| $M_1$ | *x* | 0.026 | 0.027 | 0.023 |
| $M_1$ | *z* | 0.028 | 0.027 | 0.027 |
| $M_2$ | *x* | −0.019 | −0.010 | −0.063 |
| $M_2$ | *z* | 0.024 | 0.023 | 0.016 |
| $M_3$ | *y* | −0.016 | −0.012 | −0.040 |
| $M_3$ | *z* | 0.023 | 0.011 | 0.009 |
| $O_1$ | *x* | 0.006 | 0.014 | 0.011 |
| $O_1$ | *z* | −0.026 | −0.028 | −0.020 |
| $O_2$ | *x* | 0.014 | 0.011 | 0.003 |
| $O_2$ | *z* | −0.034 | −0.036 | −0.034 |

[a] The definitions of the atoms and direction are defined in Figure 1a. The results are obtained with the B3LYP/CEP-4G level of calculation.

To see the geometrical change after the geometry relaxation, the amount of shift in the atomic position from the lattice of the MgO crystal is calculated. Table 1 shows the result for the selected atoms, defined in Figure 1a, in particular directions. Five selected atoms, $M_1$, $M_2$, $M_3$, $O_1$, and $O_2$, are classified into two groups. The atoms in the first group, $M_1$ and $O_2$, are at the periphery of the cluster and thus are adjacent to point charges. Those in the second group, $M_2$, $M_3$, and $O_1$, are not adjacent to point charges and are closer to oxygen vacancy sites. From Table 1, the largest displacement is observed for the second-group atoms that are adjacent to oxygen vacancy sites, such as atom $M_2$ in structure 5V for the *x* direction. This result coincides with a prior work by D'Ercole and Pisani. They reported that only the first-neighbor atoms of vacancies moves significantly after the geometry relaxation.[20] Here, we showed that even the largest amount of shift of 0.063 Å corresponds to only 3% of a change in atomic position with respect to the Mg$-$O distance in the crystal, 2.1056 Å. Also, the amount of shift in the atoms of the first group is even smaller. Therefore, the geometrical errors caused by the use of point charges are considered to be negligible.

**B. Perfect Crystal and Surface.** Calculated consistent charges and orbital-energy differences of the bulk MgO and MgO surface, modeled with the $5 \times 6 \times 3$ cluster and calculated with B3LYP/CEP-121G, are given in Table 2.

The values of consistent point charge are 1.50 for the bulk and 1.45 for the surface. Although MgO is considered as a nearly perfect ionic crystal, the calculated values are significantly smaller than the value expected for the perfectly ionic crystal, 2.0. Gerson and Bredow obtained a consistent point charge of $\pm$1.11 from $8 \times 8 \times 4$ and $8 \times 8 \times 5$ clusters using a semiempirical method with a Löwdin population analysis.[21] When the charge is defined according to a Löwdin- or Mulliken-type population analysis, the consistent charge seems to become significantly smaller than the formal charge value. However, a presumably better description of charge, such as a charge determined by natural-population analysis,[39] gave a charge close to $\pm$1.9.[22] The present consistent charge quantities could be an artifact of using a Mulliken-type charge for an ionic system.[40] Therefore,

***Table 2.*** Calculated Energy Differences between HOMO and the Bottom of Valence Orbitals (HOMO−$V_{bottom}$), between LUMO and HOMO (LUMO−HOMO), between the Vacuum Level and LUMO (−LUMO), and between the Vacuum Level and HOMO (−HOMO) for Bulk MgO and MgO Surface Modeled by a 5 × 6 × 3 Cluster[a]

| | point-charge type | point-charge quantity (\|e\|) | HOMO−$V_{bottom}$ (eV) | LUMO−HOMO (eV) | −LUMO (eV) | −HOMO (eV) |
|---|---|---|---|---|---|---|
| bulk | formal | 2.00 | 3.87 | 6.39 (7.99) | 2.89 (1.29) | 9.28 (9.32) |
| | consistent | 1.50 | 3.91 | 6.24 (7.41) | 1.79 (0.62) | 8.03 (8.07) |
| | exp.[1,3,4] | | 4.0∼8.5[b] | 7.4∼7.8[c] | 0.85∼1.0[d] | |
| surface | formal | 2.00 | 3.90 | 6.01 (7.48) | 2.52 (1.06) | 8.54 (8.58) |
| | consistent | 1.45 | 4.25 | 5.32 (6.52) | 1.85 (0.65) | 7.17 (7.21) |
| | exp. [11] | | | | | 6.7 ± 0.4 |

[a] The formal charge and consistent point charge were used for the energy-difference calculations. Numbers in parentheses are the empirically corrected values using eqs 1 and 2. [b] Valence-bandwidth. [c] Band gap. [d] Electron affinity.

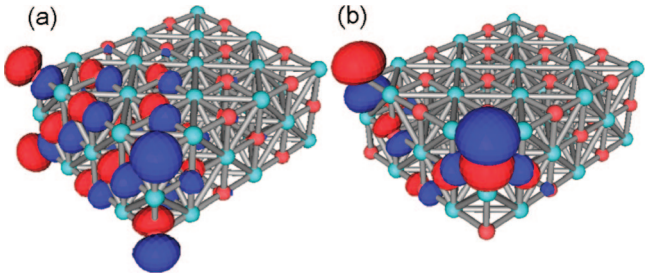


***Figure 5.*** (Color online) HOMO of 5 × 6 × 3 MgO clusters modeling (a) bulk MgO and (b) MgO surface; sky-blue (lighter) sphere, magnesium atom; red (darker) sphere, oxygen atom; blue (darker) and red (lighter) shapes, isosurface (level = 0.03) of the molecular orbital.

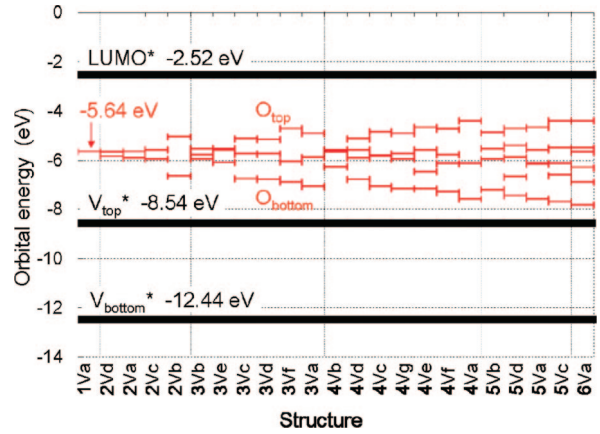


***Figure 6.*** (Color online) Distribution of orbital energies for the 24 structures defined in Figure 1b. $V_{bottom}$*, orbital energy of the bottom of valence orbitals of structure 0V; $V_{top}$*, orbital energy of the top of valence orbitals of structure 0V; LUMO*, LUMO of structure 0V; $O_{top}$, the top of oxygen-vacancy energy levels; $O_{bottom}$, the bottom of oxygen-vacancy energy levels.

calculations for systems with aggregated oxygen vacancies (subsection C) were performed using the formal charge.

The value of −HOMO in the bulk is larger than that in the surface by about 0.7−0.9 eV, as seen from Table 2. However, the difference in the other orbital-energy-related quantities between the bulk and surface is smaller. Thus, we looked at the HOMO more closely. Figure 5 shows HOMOs of the bulk MgO and the MgO surface. In both cases, the HOMO consists of oxygen 2p orbitals. In the bulk MgO (Figure 5a), the majority of oxygen 2p orbitals lie along the surface. As a consequence, interaction between neighboring oxygen atoms in the same layer has an antibonding character, while the one in the neighboring layer has a bonding character. As a sum, HOMO has an almost nonbonding character. In the MgO surface (Figure 5b), oxygen 2p orbitals stand perpendicular to the surface. The main components of the HOMO separate at the edges of the cluster, and interaction between orbitals at the edges has an antibonding character. The HOMO of the bulk MgO is therefore more stable than that of the MgO surface. The difference in HOMOs is caused by the presence/absence of point charges above the top surface of the cluster.

The empirically corrected orbital energies and experimentally observed energies[1,3,4,11] compare well. Although the calculated values are slightly underestimated in the bulk and overestimated in the surface, the degree of error from the experimental values is within a few tenths of an electronvolt.

**C. Aggregated Oxygen Vacancies at the Surface.** Figure 6 shows the distributions of orbital energies of the 24 structures shown in Figure 1b. Formal charge was used as point charge, and geometry-relaxation effects were excluded. $V_{bottom}$*, $V_{top}$*, and LUMO* are the orbital energy of the bottom of valence orbitals, that of the top of valence orbitals, and the LUMO of structure 0Va (see Figure 1b). Orbital energies shown between $V_{top}$* and LUMO* are oxygen-vacancy levels, of which the highest and lowest energies are denoted as $O_{top}$ and $O_{bottom}$, respectively, in Figure 6. Structures are sorted according to the number of oxygen vacancies. Among the structures with the same number of oxygen vacancies, structures are sorted according to the energy of $O_{bottom}$. The energy of $O_{top}$ increases, while the energy of $O_{bottom}$ decreases when the structure contains a larger number of oxygen vacancies.

In structure 1Va, the model for the surface F-center, the value of the oxygen vacancy level, $O_{Fs}$, is −5.64 eV. Experimentally, the absorption energy of the F-center is known as 5.01 eV.[5] This energy corresponds to the energy difference between the LUMO and the oxygen vacancy level. Applying eqs 1 and 2 to the $O_{Fs}$ and LUMO, respectively, leads to an energy difference of 4.51 eV, as shown in Table 3. Although the inclusion of the geometry relaxation effects would increase the current difference between the calculation and experiment by 0.4−0.5 eV as expected from Figure 4, the error of within 1 eV is still a satisfactory agreement with the experiment.

Coming back to Figure 6, among the structures with the same number of oxygen vacancies, large deviations in the energy difference between $O_{top}$ and $O_{bottom}$ ($O_{top}$−$O_{bottom}$) were observed. The $O_{top}$−$O_{bottom}$ values are relatively large for structures 2Vb, 3Vc, 3Vd, and so forth, as shown in the

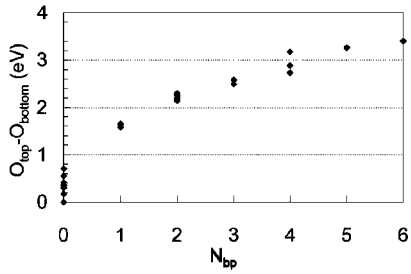


***Figure 7.*** The relationship between the number of oxygen-vacancy pairs separated by the nearest-neighbor oxygen distance and the energy difference between the top and bottom of oxygen-vacancy levels ($O_{top}-O_{bottom}$).

***Table 3.*** Orbital Energies of the LUMO and the Oxygen Vacancy Level ($O_{Fs}$) and Their Difference as well as Experimentally Measured Absorption Energy of the F Center[a]

| | LUMO | $O_{Fs}$ | LUMO-$O_{Fs}$ |
|---|---|---|---|
| uncorrected | −2.52 | −5.64 | 3.12 |
| corrected by eqs 1 and 2 | −1.06 | −5.57 | 4.51 |
| experiment | | | 5.01[5] |

[a] A B3LYP/CEP-121G calculation was performed for a MgO surface with one oxygen vacancy that traps a charge of −2 ($F_s$-center) modeled by a $Mg_{45}O_{44}$ (structure 1Va in Fig. 1b) cluster embedded in a 15 × 16 × 8 formal point-charge-box. No geometry relaxation effects were included.

gaps between red lines in Figure 6. The values of $O_{top}-O_{bottom}$ seem to be related to the number of oxygen-vacancy pairs separated by the nearest-neighbor oxygen distance, hereafter denoted as $N_{bp}$. For example, in structure 2Vd, the two oxygen vacancies are separated by more than the nearest-neighbor distance between two oxygen atoms, thus giving $N_{bp} = 0$, and the value of $O_{top}-O_{bottom}$ is about 0.2 eV. On the other hand, in structure 2Vb, the two oxygen vacancies are separated by the nearest-neighbor oxygen distance ($N_{bp} = 1$), and the value of $O_{top}-O_{bottom}$ is about 1.6 eV. To clarify this point further, the relationship between $N_{bp}$ and $O_{top}-O_{bottom}$ for all of the considered structures is plotted in Figure 7. As $N_{bp}$ increases, the $O_{top}-O_{bottom}$ value also tends to increase. Therefore, $N_{bp}$ is a convenient index to understand the orbital energy of oxygen-vacancy levels.

Figure 8 shows molecular orbitals of $O_{bottom}$ and $O_{top}$ levels for structures 2Vd and 2Vb. In structure 2Vd, the two oxygen vacancies shown by crosses are relatively far apart, and both molecular orbitals corresponding to $O_{bottom}$ (Figure 8a) and to $O_{top}$ (Figure 8b) localize at the oxygen-vacancy sites. However, in structure 2Vb, molecular orbitals corresponding to $O_{bottom}$ (Figure 8c) and to $O_{top}$ (Figure 8d) delocalize along the two oxygen vacancies. In both structures, 2Vd and 2Vb, the molecular orbital corresponding to $O_{bottom}$ shows bonding character, and that corresponding to $O_{top}$ shows antibonding character. Since those observed molecular orbitals are in the vicinity of the oxygen vacancy sites, it is possible to view these orbitals as those made by pseudoatoms. Under this viewpoint, molecular orbitals corresponding to $O_{bottom}$ and $O_{top}$ are interpreted as bonding and antibonding molecular orbitals made by two interacting pseudoatoms.

The concept of the pseudoatom was applied to the system with six oxygen vacancies, structure 6V. A pseudoatom is an electronically neutral atom representing an oxygen

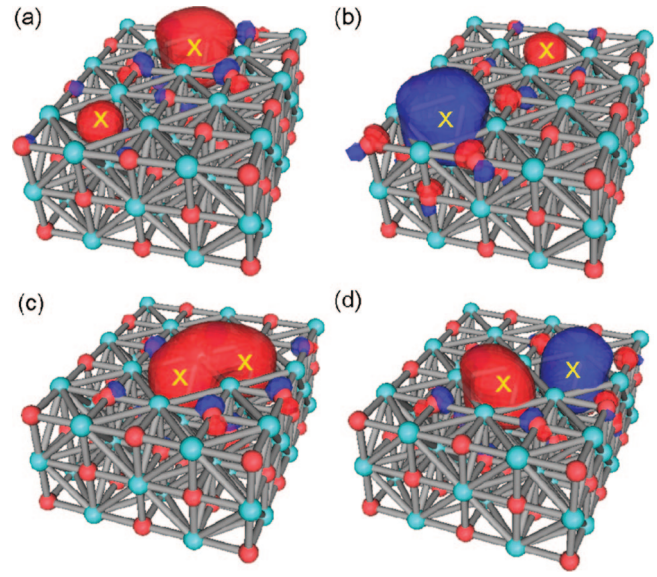


***Figure 8.*** (Color online) Molecular orbitals of the top and bottom of the oxygen-vacancy levels for structures 2Vd and 2Vb. (a) Structure 2Vd, $O_{top}$; (b) structure 2Vd, $O_{bottom}$; (c) structure 2Vb, $O_{top}$; (d) structure 2Vb, $O_{bottom}$. Sky-blue (lighter) sphere, magnesium atom; red (darker) sphere, oxygen atom; cross, oxygen-vacancy site; blue (darker) and red (lighter) shapes, isosurface (level = 0.03) of the molecular orbital.

vacancy and electrons of magnesium ions near the vacancy. The system was modeled by a cluster composed of six helium atoms. The helium atom is chosen as a representation of the pseudoatom because both a helium atom and an oxygen vacancy with a trapping charge of −2 have two electrons. In Figure 9, molecular orbitals of oxygen-vacancy levels for structure 6Va and those of the helium cluster are shown in the order of increasing orbital energy. Molecular orbitals of structure 6Va and the helium cluster have one-to-one correspondence in the correct energy ordering. The degree of delocalization differs, however, because in structure 6Va, 3s orbitals of surface magnesium atoms are dominant, while in the helium cluster, composing atomic orbitals are much more confined 1s orbitals.

It is informative to compare obtained orbital energies with those obtained using the PBC calculated by Finocchi et al.[18] They defined a unit cell of 16 atoms (4 × 4) at the surface, of which eight are oxygen sites. Their structures containing two oxygen vacancies at the surface, either homogeneously or in a close-packed manner (0.25(h) and 0.25(cp), see Figure 1 of ref 18), are compared to our structures 2Vc and 2Vb, respectively. Similarly, their structures containing four oxygen vacancies at the surface (0.5(h) and 0.5(cp)) are compared to our structures 4Vb and 4Va, respectively.

When one or more pairs of oxygen vacancies are located at the nearest-neighbor oxygen distance, as in structures 2Vb and 4Va, orbital energies agree with each other within 0.5 eV. For these systems, adjacent oxygen vacancies form extended molecular orbitals that correspond to $O_{top}$ and $O_{bottom}$. Therefore, interaction between more distant oxygen vacancies introduced by the use of the PBC does not significantly alter the oxygen-vacancy energy levels. On the other hand, when no oxygen-vacancy pairs are separated by the nearest-neighbor oxygen distance, as in structures 2Vc

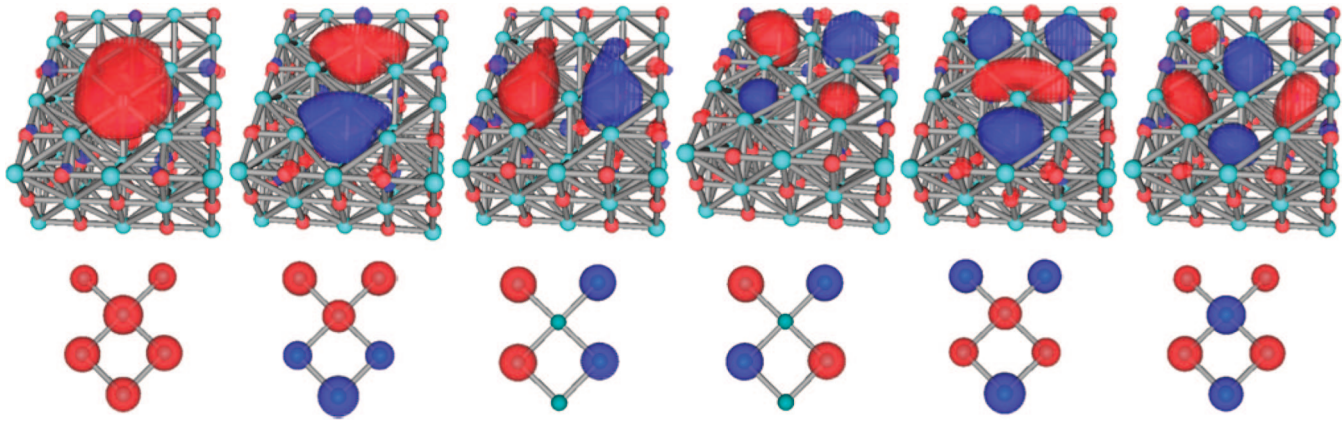

***Figure 9.*** (Color online) Molecular orbitals of oxygen-vacancy levels for structure 6V (upper row) and those of the helium cluster (lower row). In the upper row: sky-blue (lighter) sphere, magnesium atom; red (darker) sphere, oxygen atom. In the lower row: a sphere represents a helium atom; blue (darker) and red (lighter) shapes, isosurface (level = 0.03) of the molecular orbital.

and 4Vb, the difference in orbital energies enlarges to more than 0.8 eV. In this case, the sum of long-range interaction between oxygen vacancies, which is present only in the PBC model, is no longer negligible.

The PBC models a structure with oxygen vacancies periodically spread over MgO materials. This structure may be seen as annealed MgO, where oxygen vacancies evenly spread over materials. On the other hand, in the cluster model, aggregated oxygen vacancies are isolated. The considered structures may thus be seen as a locally damaged MgO surface by ion bombardment.

## Conclusions

Electronic structures of perfect bulk MgO, perfect surface MgO, an MgO surface with a surface F-center, and an MgO surface with aggregated oxygen vacancies at the surface were calculated using an embedded-cluster approach. The orbital-energy-related quantities converge within 0.3 eV when a $5 \times 6 \times 3$ cluster is used. The inclusion of geometry-relaxation effects shifts the orbital energies. However, the amount of the shift is almost irrelevant to the number of oxygen vacancies. In the calculation of perfect bulk MgO, perfect MgO surface, and an MgO surface with one oxygen vacancy, measured valence-bandwidth, band gap, and electron affinity were reproduced within a few tenths of an electronvolt of error. To achieve this accuracy, an empirical correction, accounting for the incompleteness of a basis set, on orbital energies was applied. For an MgO surface with aggregated oxygen vacancies at the surface, the distribution of energy levels corresponding to oxygen-vacancy states depends strongly on the number and configuration of oxygen vacancies. When oxygen vacancies are separated by the nearest-neighbor oxygen distance, the energy difference between the top and bottom of the oxygen-vacancy levels ($O_{top}-O_{bottom}$) becomes larger. As the number of oxygen-vacancy pairs separated by the nearest-neighbor oxygen distance increases, the value of $O_{top}-O_{bottom}$ increases. Molecular orbitals of oxygen-vacancy states largely localize in the vicinity of the vacancy sites. An oxygen-vacancy site can therefore be viewed as a pseudoatom. Molecular orbitals of the oxygen-vacancy states can be interpreted as orbitals formed by interacting pseudoatoms. Oxygen-vacancy energy levels for isolated vacancies modeled by cluster calculation and those for evenly spread vacancies modeled by PBC are similar when two vacancies are adjacent. On the other hand, when no vacancy pairs are separated by the nearest-neighbor oxygen distance, the difference in the vacancy energy levels becomes larger. It is concluded that MgO with aggregated oxygen vacancies can exhibit significantly different optical and electronic properties as compared with MgO with monovacancies or periodically distributed vacancies.

## References


(1) Aboelfotoh, M. O.; Lorenzen, J. A. Influence of Secondary-electron Emission from MgO Surfaces on Coltage-breakdown Curves in Penning Mixutures for Insulated-electrode Discharges. *J. Appl. Phys.* **1977**, *48*, 4754–4759.

(2) Motoyama, Y.; Sato, F. Calculation of Secondary Electron Emission Yield $\gamma$ from MgO Surface. *IEEE Trans. Plasma Sci.* **2006**, *34*, 336–342.

(3) Johnson, P. D. Some Optical Properties of MgO in the Vacuum Ultraviolet. *Phys. Rev.* **1954**, *94*, 845–846.

(4) Roessler, D. M.; Walker, W. C. Electronic Spectrum and Ultraviolet Optical Properties of Crystalline MgO. *Phys. Rev.* **1967**, *159*, 733–738.

(5) Chen, Y.; Kolopus, J. L.; Sibley, W. A. Luminescence of the $F^+$ Center in MgO. *Phys. Rev.* **1969**, *186*, 865–870.

(6) Williams, R. T.; Williams, J. W.; Turner, T. J.; Lee, K. H. Kinetics of Radiative Recombination in Magnesium Oxide. *Phys. Rev. B: Condens. Matter Mater. Phys.* **1979**, *20*, 1687–1699.

(7) Summers, G. P.; Wilson, T. M.; Jeffries, B. T.; Tohver, H. T.; Chen, Y.; Abraham, M. M. Luminescence from Oxygen Vacancies in MgO Crystals Thermochemically Reduced at High Temperatures. *Phys. Rev. B: Condens. Matter Mater. Phys.* **1983**, *27*, 1283–1291.

(8) Rosenblatt, G. H.; Rowe, M. W.; Williams, G. P., Jr.; Williams, R. T.; Chen, Y. Luminescence of F and $F^+$ centers in Magnesium Oxide. *Phys. Rev. B: Condens. Matter Mater. Phys.* **1989**, *39*, 10309–10318.

(9) Chaudhri, M. M.; Sands, H. S. Photoluminescence from Indented MgO Crystals Using a Near Ultraviolet/Visible Raman Microscope. *J. Appl. Phys.* **1997**, *82*, 785–791.

(10) González, R.; Monge, M. A.; Munos Santiuste, J. E.; Pareja, J. E.; Chen, Y.; Kotomin, E.; Kukla, M. M.; Popov, A. I. Photoconversion of F-type Centers in Thermochemically

Reduced MgO Single Crystals. *Phys. Rev. B: Condens. Matter Mater. Phys.* **1999**, *59*, 4786–4790.

(11) Kantorovich, L. N.; Shluger, A. L.; Sushko, P. V.; Günster, J.; Stracke, P.; Goodman, D. W.; Kempter, V. Mg Clusters on MgO surfaces: Study of the Nucleation Mechanism with MIES and Ab Initio Calculations. *Faraday Discuss.* **1999**, *114*, 173–194.

(12) Wang, Q. S.; Holzwarth, N. A. W. Electronic Structure of Vacancy Defects in MgO Crystals. *Phys. Rev. B: Condens. Matter Mater. Phys.* **1990**, *41*, 3211–3225.

(13) Gibson, A.; Haydock, R.; LaFemina, J. P. The Electronic Structure of Neutral and Charged Surface Vacancy Defects in Periclase. *Appl. Surf. Sci.* **1993**, *72*, 285–293.

(14) Gibson, A.; Haydock, R.; LaFemina, J. P. Stability of Vacancy Defects in MgO: The Role of Charge Neutrality. *Phys. Rev. B: Condens. Matter Mater. Phys.* **1994**, *50*, 2582–2592.

(15) Castanier, E.; Noguera, C. Non-stoichiometric Reconstructions on MgO(100). *Surf. Sci.* **1996**, *364*, 17–29.

(16) Scorza, E.; Birkenheuer, U.; Pisani, C. The Oxygen Vacancy at the Surface and in Bulk MgO: An Embedded-Cluster study. *J. Chem. Phys.* **1997**, *107*, 9645–9657.

(17) Orlando, R.; Millini, R.; Perego, G.; Dovesi, R. Catalytic Properties of F-centres at the Magnesium Oxide Surface: Hydrogen Abstraction from Methane. *J. Mol. Catal.* **1997**, *119*, 253–262.

(18) Finocchi, F.; Goniakowski, J.; Noguera, C. Interaction between Oxygen Vacancies on MgO(100). *Phys. Rev. B: Condens. Matter Mater. Phys.* **1999**, *59*, 5178–5188.

(19) D'Ercole, A.; Giamello, E.; Pisani, C.; Ojämae, L. Embedded-Cluster Study of Hydrogen Interaction with an Oxygen Vacancy at the Magnesium Oxide Surface. *J. Phys. Chem. B* **1999**, *103*, 3872–3876.

(20) D'Ercole, A.; Pisani, C. Ab Initio Study of Hydrogen Dissociation at a Surface Divancacy on the (001) MgO Surface. *J. Chem. Phys.* **1999**, *111*, 9743–9753.

(21) Gerson, A. R.; Bredow, T. MgO(100) Surface Relaxation and Vacancy Defects: a Semi-Empirical Quantum-Chemical Study. *Phys. Chem. Chem. Phys.* **1999**, *1*, 4889–4896.

(22) Sushko, P. V.; Shluger, A. L.; Catlow, C. R. A. Relative Energies of Surface and Defect States: Ab Initio Calculations for the MgO (001) Surface. *Surf. Sci.* **2000**, *450*, 153–170.

(23) Sushko, P. V.; Gavartin, J. L.; Shluger, A. L. Electronic Properties of Structural Defects at the MgO (001) Surface. *J. Phys. Chem. B* **2002**, *106*, 2269–2276.

(24) Montanari, B.; Civalleri, B.; Zicovich-Wilson, C. M.; Dovesi, R. Properties, Dynamics, and Electronic Structure of Condensed Systems and Clusters Influence of the Exchange-Correlation functional in All-Electron Calculations of Vibrational Frequencies of Corundum ($Al_2O_3$). *Int. J. Quantum Chem.* **2006**, *106*, 1703–1714.

(25) Becke, A. D. Density-Functional Thermochemistry. III. The Role of Exact Exchange. *J. Chem. Phys.* **1993**, *98*, 5648–5652.

(26) Lee, C.; Yang, W.; Parr, R. G. Development of the Colle-Salvetti Correlation-Energy Formula into a Functional of the Electron Density. *Phys. Rev. B: Condens. Matter Mater. Phys.* **1988**, *37*, 785–789.

(27) Ladik, J.; Bogar, F.; Penke, B. Comparison of HF, HF+MP2, LDA, BLYP and B3LYP Band Structures of the Homopeptides. *Int. J. Quantum Chem.* **2004**, *98*, 522–527.

(28) Yang, S.; Kertesz, M. Bond Length Alternation and Energy Band Gap of Polyyne. *J. Phys. Chem. A* **2006**, *110*, 9771–9774.

(29) Perger, W. F. Calculation of Band Gaps in Molecular Crystals Using Hybrid Functional Theory. *Chem. Phys. Lett.* **2003**, *368*, 319–323.

(30) Muscat, J.; Wander, A.; Harrison, N. M. On the Prediction of Band Gaps from Hybrid Functional Theory. *Chem. Phys. Lett.* **2001**, *342*, 397–401.

(31) Xu, X.; Nakatsuji, H.; Ehara, M.; Lü, X.; Wang, N. Q.; Zhang, Q. E. Cluster Modeling of Metal Oxides: the Influence of the Surrounding Point Charges on the Embedded Cluster. *Chem. Phys. Lett.* **1998**, *292*, 282–288.

(32) Lü, X.; Xu, X.; Wang, N.; Zhang, Q.; Ehara, M.; Nakatsuji, H. Cluster Modeling of Metal Oxides: How to Cut out a Cluster. *Chem. Phys. Lett.* **1998**, *291*, 445–452.

(33) Rappe, A. K.; Casewit, C. J.; Colwell, K. S.; Goddard, W. A., III; Skiff, W. M. UFF, a Full Periodic Table Force Field for Molecular Mechanics and Molecular Dynamics Simulations. *J. Am. Chem. Soc.* **1992**, *114*, 10024–10035.

(34) Stevens, W. J.; Basch, H.; Krauss, M. Compact Effective Potentials and Efficient Shared-Exponent Basis Sets for the First- and Second-row Atoms. *J. Chem. Phys.* **1984**, *81*, 6026–6033.

(35) Zhan, C.-G.; Nichols, J. A.; Dixon, D. A. Ionization Potential, Electron Affinity, Electronegativity, Hardness, and Electron Excitation Energy: Molecular Properties from Density Functional Theory Orbital Energies. *J. Phys. Chem. A* **2003**, *107*, 4184–4195.

(36) Salzner, U.; Lagowski, J. B.; Pickup, P. G.; Poirier, R. A. Design of Low Band Gap Polymers Employing Density Functional Theory — Hybrid Functionals Ameliorate Band Gap Problem. *J. Comput. Chem.* **1998**, *18*, 1943–1953.

(37) Takahata, Y.; Chong, D. P. Density-Functional Calculations of Molecular Electron Affinities. *J. Braz. Chem. Soc.* **1999**, *10*, 354–358.

(38) Frisch, M. J.; Trucks, G. W.; Schlegel, H. B.; Scuseria, G. E.; Robb, M. A.; Cheeseman, J. R.; Montgomery, J. A., Jr.; Vreven, T.; Kudin, K. N.; Burant, J. C.; Millam, J. M.; Iyengar, S. S.; Tomasi, J.; Barone, V.; Mennucci, B.; Cossi, M.; Scalmani, G.; Rega, N.; Petersson, G. A.; Nakatsuji, H.; Hada, M.; Ehara, M.; Toyota, K.; Fukuda, R.; Hasegawa, J.; Ishida, M.; Nakajima, T.; Honda, Y.; Kitao, O.; Nakai, H.; Klene, M.; Li, X.; Knox, J. E.; Hratchian, H. P.; Cross, J. B.; Bakken, V.; Adamo, C.; Jaramillo, J.; Gomperts, R.; Stratmann, R. E.; Yazyev, O.; Austin, A. J.; Cammi, R.; Pomelli, C.; Ochterski, J. W.; Ayala, P. Y.; Morokuma, K.; Voth, G. A.; Salvador, P.; Dannenberg, J. J.; Zakrzewski, V. G.; Dapprich, S.; Daniels, A. D.; Strain, M. C.; Farkas, O.; Malick, D. K.; Rabuck, A. D.; Raghavachari, K.; Foresman, J. B.; Ortiz, J. V.; Cui, Q.; Baboul, A. G.; Clifford, S.; Cioslowski, J.; Stefanov, B. B.; Liu, G.; Liashenko, A.; Piskorz, P.; Komaromi, I.; Martin, R. L.; Fox, D. J.; Keith, T.; Al-Laham, M. A.; Peng, C. Y.; Nanayakkara, A.; Challacombe, M.; Gill, P. M. W.; Johnson, B.; Chen, W.; Wong, M. W.; Gonzalez, C.; Pople, J. A. *Gaussian 03*, revision D.02; Gaussian, Inc., Wallingford, CT, 2004.

(39) Reed, A. E.; Weinstock, R. B.; Weinhold, F. Natural Population Analysis. *J. Chem. Phys.* **1985**, *83*, 735–746.

(40) Collins, J. B.; Streitwieser, A. Integrated Spatial Electron Populations in Molecules: Application to Simple Molecules. *J. Comput. Chem.* **1980**, *1*, 81–87.

CT700303V